Generation of partially coherent vortex bottle beams

Lianzhou Rao (饶连周)[1,2] and Jixiong Pu (蒲继雄)[1]

[1]*Department of Electronic Science & Technology, Huaqiao University, Quanzhou 362021*

[2]*Department of Physics and Electromechanical Engineering, Sanming University, Sanming 365004*

Received January 4, 2007

Intensity distribution of the partially coherent Bessel vortex beams focused by an aperture lens is investigated. It is found that the intensity distribution in the neighborhood of the geometrical focus is not only dependent on the topological charge and the radial frequency of the incident partially coherent Bessel vortex beam, but also on its coherence length. Based on this, the desired partially coherent vortex bottle beams can be obtained by choosing appropriate values of parameters. Because such bottle beams possess characteristics of low coherence and vortex, it may be used in microscopic particles guiding, trapping, and inducing rotation.

OCIS codes: 050.1970, 030.1640, 999.9999 (vortex bottle beam).

In recent years, there have been increasing interests in the generation of an optical bottle beam, in which a dark focus is surrounded by regions of higher intensity[1−11]. Various applications of a bottle beam in atom guiding, atom trapping, and optical tweezers have been explored[1−3]. In a blue-detuned bottle beam, the atoms are guided to the dark or the low-field region and manipulated in the dark center[1], and the storage time can approach the order of 1 s[3]. Several techniques for generating an optical bottle beam were also described. Kaplan *et al.* proposed a new scheme for constructing a single-beam dark optical trap that minimizes light-induced perturbations of the trapped atoms[6]. Yelin *et al.* presented an optical setup for generating three-dimensional (3D) dark focus[7]. Recently, a new method for generating partially coherent bottle beams has been presented[8]. In addition, it is well recognized that an optical vortex beam with a helical phase structure of $\exp(in\phi)$, where n represents the topological charge and ϕ is the azimuthal angle, carries orbital angular momentum (OAM)[12]. Such beam was also applied to induce rotation of particles due to the transfer of OAM from the light to the particles[13]. Here, we notice that all the techniques for generating partially coherent bottle beams above do not take into account the beams carrying optical vortex. Can partially coherent vortex bottle beams be generated by focused partially coherent high order Bessel vortex beams? This question is interesting, because the vortex bottle beams of low coherence may show some advantages over those of complete coherence[14] and possess the characteristics of the optical vortex. In this letter, we present a novel method for generation of partially coherent vortex bottle beams. It is shown that the size of dark focus is adjustable by modulating the spatial coherence length and the topological charge etc..

Suppose that a partially coherent high order Bessel vortex beam is incident upon an aperture lens with full width $2a$ and focal length f at the $z = -f$ plane, as shown in Fig. 1. The field distribution of the high order Bessel vortex beams in the polar coordinate system is written as[15,16]

$$E^{(0)}(\mathbf{r},\omega) = E_0 J_n(\alpha r)\exp(in\phi)\exp(i\omega t)\exp(i\beta),$$
$$n = 1, 2, 3, \cdots, \quad (1)$$

where J_n is the nth-order Bessel function of the first kind, $\mathbf{r}$ is the position vector of a point p in the aperture lens, α is a radial frequency, and β is an arbitrary phase (as a spatially distributed random variable).

The cross-spectral density of a partially coherent wave field can be written as

$$W^{(0)}(\mathbf{r}_1,\mathbf{r}_2,\omega) = \langle E^*(\mathbf{r}_1,\omega)E(\mathbf{r}_2,\omega)\rangle, \quad (2)$$

where the angle bracket denotes an ensemble average monochromatic realization of the field. Substituting Eq. (1) into Eq. (2) and using Gaussian-Schell coherent model[17], we obtain the expression for the cross-spectral density in the $z = -f$ plane

$$W^{(0)}(\mathbf{r}_1,\mathbf{r}_2,z=-f) = E_0^2 J_n(\alpha r_1) J_n(\alpha r_2)$$
$$\times \exp\left[-(\mathbf{r}_1-\mathbf{r}_2)^2 \Big/ 2\sigma^2\right]\exp\left[-in(\phi_1-\phi_2)\right], \quad (3)$$

where σ is the transverse coherence length, E_0 the constant amplitude factor.

According to the generalized Huygens-Fresnel diffraction integral, the cross-spectral density in the focused field can be expressed as[17]

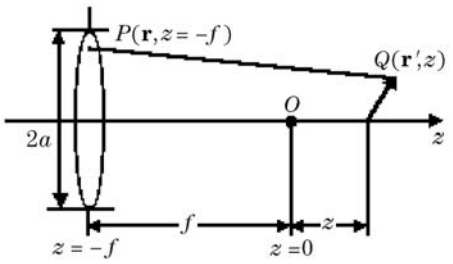

Fig. 1. Notation relating to the aperture-lens system.

1671-7694/2007/070379-04

$$W(r_1', r_2', \phi_1', \phi_2', z) = E_0^2 \left(\frac{k}{2\pi B}\right)^2 \exp\left[-\frac{ikD}{2B}(r_1'^2 - r_2'^2)\right]$$
$$\times \int_0^a \int_0^a \int_0^{2\pi} \int_0^{2\pi} \exp\left[\frac{-(r_1^2 + r_2^2)}{2\sigma^2}\right]$$
$$\times \exp\left[-\frac{ikA}{2B}(r_1^2 - r_2^2)\right] \exp\left[\frac{ikr_1' r_1}{B}\cos(\phi_1' - \phi_1)\right]$$
$$\times \exp\left[-\frac{ikr_2' r_2}{B}\cos(\phi_2' - \phi_2)\right]$$
$$\times J_n(\alpha r_1) J_n(\alpha r_2) \exp\left[\frac{r_1 r_2 \cos(\phi_1 - \phi_2)}{\sigma^2}\right]$$
$$\times \exp[-in(\phi_1 - \phi_2)] r_1 r_2 \mathrm{d}r_1 \mathrm{d}r_2 \mathrm{d}\phi_1 \mathrm{d}\phi_2, \quad (4)$$

where $k = 2\pi/\lambda$ is the wave number, and the integral is over the whole aperture. A, B, C, and D are elements of the following matrix $ABCD$

$$\begin{pmatrix} A & B \\ C & D \end{pmatrix} = \begin{pmatrix} -z/f & z+f \\ -1/f & 1 \end{pmatrix}. \quad (5)$$

By use of the following formulae[18,19]

$$\exp\left[\frac{ikr'r}{B}\cos(\phi' - \phi)\right]$$
$$= \sum_{l=-\infty}^{\infty} i^l J_l\left(\frac{kr'r}{B}\right) \exp[il(\phi' - \phi)], \quad (6)$$

$$\int_0^{2\pi} \exp\left[-in\phi_1 + \frac{r_1 r_2}{\sigma^2}\cos(\phi_1 - \phi_2)\right] \mathrm{d}\phi_1$$
$$= 2\pi \exp(-in\phi_2) I_n\left(\frac{r_1 r_2}{\sigma^2}\right), \quad (7)$$

$$\int_0^{2\pi} \exp(im\phi)\mathrm{d}\phi = \begin{cases} 2\pi & \text{if } m = 0 \\ 0 & \text{if } m \neq 0 \end{cases}, \quad (8)$$

we obtain the expression for the cross-spectral density of the focused field

$$W(r_1', r_2', \phi_1', \phi_2', z) = E_0^2 \left(\frac{k}{B}\right)^2 \exp\left[-\frac{ikD}{2B}(r_1'^2 - r_2'^2)\right]$$
$$\times \sum_{l=-\infty}^{\infty} \int_0^a \int_0^a \exp\left[\frac{-(r_1^2 + r_2^2)}{2\sigma^2}\right] \exp\left[-\frac{ikA}{2B}(r_1^2 - r_2^2)\right]$$
$$\times J_n(\alpha r_1) J_n(\alpha r_2) J_l\left(\frac{kr_1' r_1}{B}\right) J_l\left(\frac{kr_2' r_2}{B}\right)$$
$$\times I_{|l+n|}\left(\frac{r_1 r_2}{\sigma^2}\right) \exp[il(\phi_1' - \phi_2')] r_1 r_2 \mathrm{d}r_1 \mathrm{d}r_2. \quad (9)$$

Here, letting $r_1' = r_2' = r'$, $\phi_1' = \phi_2' = \phi'$ in Eq. (9), the analytical expression for the intensity distribution of the focused field is given by

$$I(\rho', \Delta z) = 4\pi^2 E_0^2 \left(\frac{N}{\Delta z + 1}\right)^2$$
$$\times \sum_{l=-\infty}^{\infty} \sum_{m=0}^{\infty} \left\{ \frac{\left(1/2\sigma_{\mathrm{g}}^2\right)^{|n+l|+2m}}{m!\Gamma\left(|n+l|+m+1\right)} \right.$$
$$\times \left[\int_0^1 \rho^{|n+l|+2m+1} \exp\left(-\frac{\rho^2}{2\sigma_{\mathrm{g}}^2}\right) J_n\left(\alpha N\sqrt{\lambda f}\rho\right) \right.$$
$$\left. \times J_l\left(\frac{2\pi N\rho'\rho}{\Delta z + 1}\right) \cos\left(\frac{\pi N\rho^2}{1 + 1/\Delta z}\right) \mathrm{d}\rho\right]^2$$
$$+ \left[\int_0^1 \rho^{|n+l|+2m+1} \exp\left(-\frac{\rho^2}{2\sigma_{\mathrm{g}}^2}\right) J_n\left(\alpha N\sqrt{\lambda f}\rho\right) \right.$$
$$\left. \left. \times J_l\left(\frac{2\pi N\rho'\rho}{\Delta z + 1}\right) \sin\left(\frac{\pi N\rho^2}{1 + 1/\Delta z}\right) \mathrm{d}\rho\right]^2 \right\}, \quad (10)$$

where $\rho' = r'/a$ and $\rho = r/a$ are relative polar radius, $\Delta z = z/f$ is relative axial distance, $\Gamma\left(|n+l|+m+1\right)$ is the gamma function, $N = a^2/\lambda f$ is the Fresnel number viewed from the geometrical focus, and $\sigma_{\mathrm{g}} = \sigma/a$ is the normalized coherence length. From Eq. (10), We find that the intensity distribution of the focused field depends on the radial frequency α, Fresnel number N, normalized coherence length σ_{g}, and topological charge n.

Based on above equations, we can perform the numerical calculation. By choosing the suitable values of α, σ_{g}, and n, we may achieve the desired intensity distribution near the focus. Figures 2(a)—(d) give the intensity distribution near the geometrical focus for different topological charges n ($n = 1, 2, 3$, and 4, respectively). In Fig. 2, the more whiteness indicates the higher intensity (the same applies to the other figures). We find that a dark focus surrounded by higher intensities is achieved. The beam having this kind of dark focus is called a bottle beam. Since the incident beam is partially coherent and

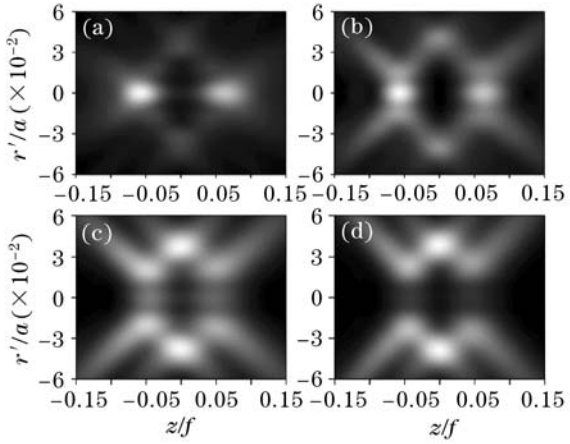

Fig. 2. Simulation for the optical field distribution near the geometrical focus for different values of topological charge n. (a) $n = 1$, (b) $n = 2$, (c) $n = 3$, (d) $n = 4$. $\alpha = 1$, $\sigma_{\mathrm{g}} = 0.5$, and other parameters are $f = 100$ mm, $\lambda = 0.6328$ μm, $N = 40$.

carrying optical vortex, the generated beam with a dark focus may appropriately be called a partially coherent vortex bottle beam. Figure 2 shows that both transverse and longitudinal dimensions of the dark focus change with the increment of the topological charge n. The transverse intensity surrounding the dark focus increases and the longitudinal intensity surrounding the dark focus decreases with the increase of n, respectively.

In Figs. 3(a)—(d), we plot the intensity distribution near the geometrical focus for different values of the normalized coherence length σ_g ($\sigma_g = 0.8, 1.5, 2$, and 2.5, respectively). The topological charge is chosen as $n = 1$. We readily find that both transverse and longitudinal dimensions of the dark focus increase lentamente with the increment of σ_g. It is also found that the transverse intensity surrounding the dark focus increases and the longitudinal intensity surrounding the dark focus decreases with the increase of σ_g, respectively. Especially, for the high coherence (see Fig. 3(d)) or the large topological charge case (see Fig. 2(d)), the intensity ring surrounding the dark focus produces a pair of low-intensity gaps in the axis. Based on this characteristic, we may present a novel approach that the atoms are guided from the low-intensity gaps to the dark focus region and can be trapped in the dark center by decreasing the σ_g.

In Figs. 4(a)—(d), we plot the intensity distribution near the geometrical focus for different values of the radial frequency α ($\alpha = 0.5, 0.8, 1$, and 1.5, respectively). It is found that both transverse and longitudinal dimensions of the dark focus increase with the increment of α. This property can also be used to control the dimensions of the dark focus. Especially, for the case of $\alpha = 0.5$ (see Fig. 4(a)), the intensity surrounding the dark focus is much more uniform than for other case. The transverse size D_r and the longitudinal size D_z of the dark focus as a function of σ_g for different values of α are presented in Fig. 5. It is shown that for a fixed σ_g, the larger the value of α is, the wider the transverse size of the dark focus is, and also the longitudinal size is; and for a fixed α and $\sigma_g \geq 0.5$, the transverse size and the longitudinal size of the dark focus change lentamente or keep invariance with the increment of σ_g.

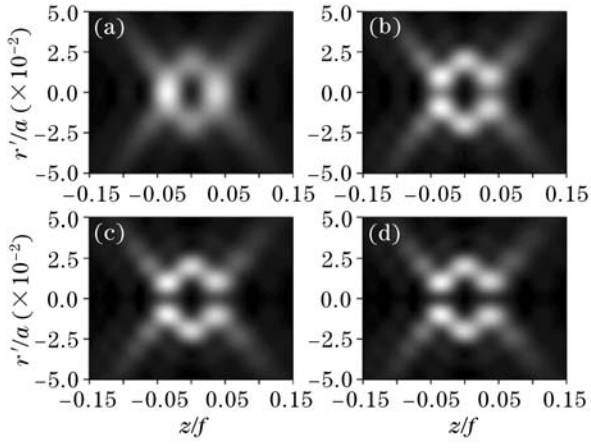

Fig. 3. Simulation for the optical field distribution near the geometrical focus for different degrees of coherence σ_g. (a) $\sigma_g = 0.8$, (b) $\sigma_g = 1.5$, (c) $\sigma_g = 2$, (d) $\sigma_g = 2.5$. $\alpha = 0.5$, $n = 1$, other parameters are the same as in Fig. 2.

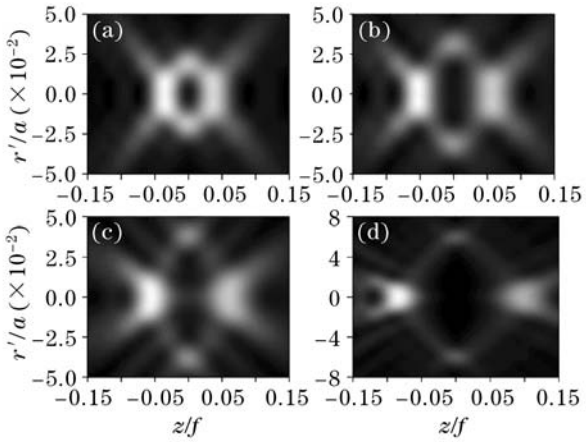

Fig. 4. Simulation for the optical field distribution near the geometrical focus for different radial frequencies α. (a) $\alpha = 0.5$, (b) $\alpha = 0.8$, (c) $\alpha = 1$, (d) $\alpha = 1.5$. $\sigma_g = 1$, $n = 1$, other parameters are the same as in Fig. 2.

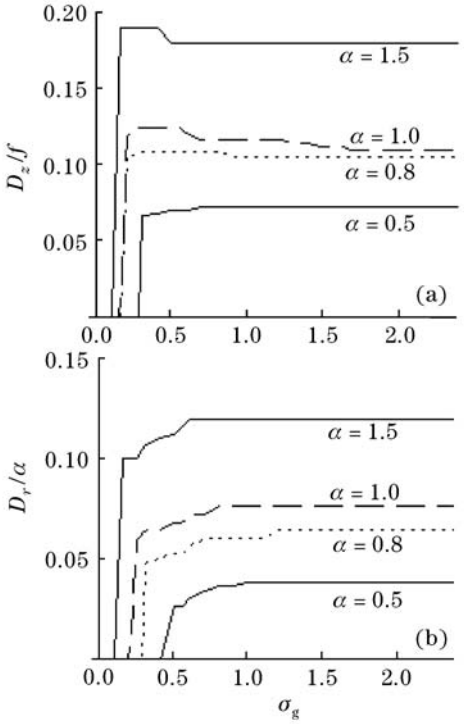

Fig. 5. Longitudinal size D_z and transverse size D_r of the dark focus as functions of σ_g for different radial frequencies α. $n = 1$, other parameters are the same as in Fig. 2.

The behaviors of the intensity distribution mentioned above can be understood easily. It is known that the dark vortex core (i.e., the dark core of the intensity profiles) in the focal region increases with increasing σ_g or n, and for low coherence case, the core fills with diffuse light[15,16,19]. As shown above, for the $\sigma_g < 0.4$ case (see Fig. 5, $n = 1$), the dark focus disappeared. However, with increasing σ_g or n, the vortex bottle beam and its low-intensity gaps in the optical axis can be generated in the focal region.

In conclusion, we have investigated the 3D intensity distribution of the partially coherent Bessel vortex beams focused by an aperture lens. It has been shown that the intensity distribution in the neighborhood of the geomet-

rical focus is not only dependent on the topological charge and the radial frequency of the incident partially coherent Bessel vortex beam, but also on its coherence length. Based on this point, a novel method was presented for achieving a dark focus surrounded by higher intensity. Namely, by modulating the coherence length, radial frequency, and the topological charge, we can produce the dark focus of desired size. It is well known that partially coherent Bessel vortex beams possess some advantages, such as low sensitivity to speckle and vortex characteristic etc.. Therefore, the generated dark focus may be used in microscopic particles guiding, trapping, and inducing rotation.

This work was supported by the National Natural Science Foundation of China (No. 60477041), the Natural Science Project of the Education Bureau of Fujian Province (No. JA06048), and the Natural Science Project of Sanming University (No. B0603/G). J. Pu is the author to whom the correspondence should be address, his e-mail address is jixiong@hqu.edu.cn.

References

1. A. Ashkin, J. M. Dziedzic, J. E. Bjorkholm, and S. Chu, Opt. Lett. **11,** 288 (1986).
2. J. Yin and Y. Zhu, J. Appl. Phys. **85,** 2473 (1999).
3. R. Ozeri, L. Khaykovich, and N. Davidson, Phys. Rev. A **59,** 1750 (1999).
4. J. Arlt and M. J. Padgett, Opt. Lett. **25,** 191 (2000).
5. T. Freegrade and K. Dholakia, Phys. Rev. A **66,** 013413 (2000).
6. A. Kaplan, N. Friedman, and N. Davidson, J. Opt. Soc. Am. B **19,** 1233 (2002).
7. D. Yelin, B. E. Bouma, and G. J. Tearney, Opt. Lett. **29,** 661 (2004).
8. J. Pu, X. Liu, and S. Nemoto, Opt. Commun. **252,** 7 (2005).
9. D. McGloin, G. C. Spalding, H. Melville, W. Sibbett, and K. Dholakia, Opt. Commun. **225,** 215 (2003).
10. B. P. S. Ahluwalia, X.-C. Yuan, and S. H. Tao, Opt. Commun. **238,** 177 (2004).
11. Y. Chen, J. Pu, and X. Liu, Chin. J. Lasers (in Chinese) **33,** 1375 (2006).
12. L. Allen, M. W. Beijersbergen, R. J. C. Spreeuw, and J. P. Woerdman, Phy. Rev. A **45,** 8185 (1992).
13. M. Gao, C. Gao, and Z. Lin, Chin. Opt. Lett. **5,** 89 (2007).
14. J. Pu, S. Nemoto, and X. Liu, Appl. Opt. **43,** 5281 (2004).
15. D. M. Palacios, I. D. Maleev, A. S. Marathay, and G. A. Swartzlander, Jr., Phys. Rev. Lett. **92,** 143905 (2004).
16. I. D. Maleev, D. M. Palacios, A. S. Marathay, and G. A. Swartzlander, Jr., J. Opt. Soc. Am. B **21,** 1895 (2004).
17. L. Mandel and E. Wolf, *Optical Coherence and Quantum Optics* (Cambridge University Press, Cambridge, 1995).
18. V. Jarutis, R. Paškauskas, and A. Stabinis, Opt. Commun. **184,** 105 (2000).
19. L. E. Helseth, Opt. Commun. **229,** 85 (2004).